Biophysical Journal
Article

Biophysical Society

Association of Endophilin B1 with Cytoplasmic Vesicles

Jinhui Li,[1] Barbara Barylko,[3] John P. Eichorst,[1] Joachim D. Mueller,[2] Joseph P. Albanesi,[3] and Yan Chen[1,*]
[1]Department of Physics and [2]School of Physics and Astronomy, University of Minnesota, Minneapolis, Minnesota; and [3]UT Southwestern Medical Center, Dallas, Texas

ABSTRACT Endophilins are SH3- and BAR domain-containing proteins implicated in membrane remodeling and vesicle formation. Endophilins A1 and A2 promote the budding of endocytic vesicles from the plasma membrane, whereas endophilin B1 has been implicated in vesicle budding from intracellular organelles, including the *trans*-Golgi network and late endosomes. We previously reported that endophilins A1 and A2 exist almost exclusively as soluble dimers in the cytosol. Here, we present results of fluorescence fluctuation spectroscopy analyses indicating that, in contrast, the majority of endophilin B1 is present in multiple copies on small, highly mobile cytoplasmic vesicles. Formation of these vesicles was enhanced by overexpression of wild-type dynamin 2, but suppressed by expression of a catalytically inactive dynamin 2 mutant. Using dual-color heterospecies partition analysis, we identified the epidermal growth factor receptor on endophilin B1 vesicles. Moreover, a proportion of endophilin B1 vesicles also contained caveolin, whereas clathrin was almost undetectable on those vesicles. These results raise the possibility that endophilin B1 participates in dynamin 2-dependent formation of a population of transport vesicles distinct from those generated by A-type endophilins.

INTRODUCTION

Endophilins are 40–50 kDa peripheral membrane proteins implicated in sensing and inducing membrane curvature during vesicle formation (1). Although divided into three classes (A, B, and C) based on their amino acid sequences, all endophilins share a common domain composition, including an N-terminal amphipathic helix (termed Helix-0) followed by a Bin/amphiphysin/Rvs domain, a variable-length linker region, and a C-terminal Src Homology 3 (SH3) domain. The Bin/amphiphysin/Rvs domains homodimerize into crescent-shaped structures, creating positively charged concave surfaces that interact with negatively charged phospholipids in membranes (2–5). Helix-0 penetrates the lipid bilayer and is apparently essential for membrane binding (6–9).

Endophilin A1 (EndoA1) is the best characterized member of the endophilin family, primarily due to its critical role in synaptic vesicle recycling (10). It interacts via its SH3 domain with dynamin (Dyn), a large (~100 kDa) GTPase that catalyzes membrane scission, and with synaptojanin, a phosphoinositide phosphatase required for uncoating of clathrin-coated vesicles (11,12). The precise function of EndoA1 in the membrane vesiculation process is not entirely understood. Its ability to induce membrane curvature (2) and scission (13) in vitro suggests that it may carry out similar activities on the plasma membrane of cells. Indeed, disruption of EndoA1 function or expression resulted in defective synaptic vesicle recycling and an increase in the number of clathrin-coated pits in a variety of experimental systems (14–17). However, knockout of all three type A endophilins in mice increased the number of clathrin-coated vesicles in synapses without affecting the number of clathrin-coated pits (18). This surprising result indicates that, at least in mouse synapses, endophilin is not essential for inducing membrane curvature or scission but instead functions cooperatively with synaptojanin in the uncoating process (18,19). In contrast to EndoA1, which participates largely in clathrin-dependent pathways, endophilin A2 (EndoA2) has recently been implicated vesicle formation during clathrin-independent endocytosis (20,21).

Whereas the class A endophilins function primarily on the plasma membrane, endophilin B1 (EndoB1) is concentrated on internal membranes (22) and has been linked to intracellular trafficking pathways, including those involving mitochondria, endosomes, and the *trans*-Golgi network. Endo B1 was independently identified by two groups in screens for binding partners of Bax, a protein that induces mitochondrial pore formation during apoptosis (23,24).

Submitted August 19, 2015, and accepted for publication June 16, 2016.
*Correspondence: chen@physics.umn.edu
Editor: Paul Wiseman.
http://dx.doi.org/10.1016/j.bpj.2016.06.017

Hence, the protein is also referred to as Bif-1 (Bax interacting factor 1). Endogenous EndoB1 has been localized by immunofluorescence staining to the Golgi complex (25), mitochondria (26–28), and Rab7-positive late endosomes (29,30). Functional studies have implicated EndoB1 in vesicle budding from the *trans*-Golgi network and degradative endocytosis of the epidermal growth factor (EGF) receptor (31). However, it has been best characterized for its roles in autophagy and apoptosis (32–34).

We previously showed that EndoA2 exists almost exclusively as a single, dimeric species in the cytosol of living cells (35). In this study, we used a variety of fluorescence fluctuation spectroscopy (FFS) analysis techniques to examine the properties of EndoB1. Autocorrelation analysis (36) and brightness analysis (37) both revealed the existence of two distinct species of EndoB1, including a cytosolic, soluble fraction, and a much larger pool associated with small intracellular vesicles. Unlike our previous study that was limited to the detection of proteins associated with cellular vesicles, this work seeks to identify changes in the labeled vesicle population that occur as a result of a deliberate perturbation. We found that the mean-binned brightness versus protein concentration provides a suitable measure for detecting changes in the brightness or concentration of the labeled vesicle fraction. We gain additional insight by performing brightness spike analysis, which identifies if a gain in brightness is associated with an increase in the labeled vesicles population. By applying these methods, we found that the formation of these EndoB1-containing vesicles was dependent on the GTPase activity of dynamin 2 (Dyn2). Using dual-color heterospecies partition analysis (HSP) (38), we identified the epidermal growth factor receptor (EGFR) on EndoB1-containing structures, confirming that these structures were bounded by membrane bilayers. In addition, a substantial proportion of EndoB1 vesicles also contained caveolin, whereas clathrin was almost undetectable on those vesicles. This study suggests that EndoB1 may be involved in the intracellular EGFR and caveolin trafficking pathways.

MATERIALS AND METHODS

Constructs and cell transfection

GFP-EndoA2, rat Dyn2-mCherry, rat Dyn2(K44A)-mCherry, and Clathrin light chain (CLC)-mCherry were cloned as previously described (35,39). EGFR-EGFP was a gift from Alexander Sorkin (Dept. of Cell Biology, University of Pittsburgh) and was previously characterized in (40). Human EndoB1 (accession number NM_016009), and Human caveolin 1 (CAV1) (accession number BC009684) were introduced into either pEGFP-N1 or pmCherry-N1 plasmid (Clontech, Mountain View, CA) at an *XhoI* and an *EcoRI* sites. pEGFPC1-epsin1 was purchased from Addgene (#22228) (Cambridge, MA). U2OS cells were obtained from American Type Culture Collection (ATCC) (Manassas, VA) and maintained in 10% fetal bovine serum and Dulbecco's modified Eagle's medium (DMEM) media. Transfection was carried out using TransFectin reagent (Bio-Rad, Hercules, CA) according to the manufacturer's instructions 24 h before measurement. EGF was purchased from Sigma-Aldrich (St Louis, MO). EGF stock solution was prepared according to the manufacturer's instructions. For the EGF assay, cells were incubated with Dulbecco's modified Eagle's medium serum-free medium for at least 4 h. Cells were treated with either 100 ng/ml or 1.5 ng/ml EGF, then incubated for 0.5 h before measurements.

Instrumentation

Fluorescence fluctuation experiments were carried out using a modified Zeiss Axiovert 200 microscope (Thornwood, NY) as previously described (41). A mode-locked Ti:sapphire laser (Tsunami, Spectra-Physics, Mountain View, CA) pumped by an intracavity doubled Nd:YVO_4 laser (Millenia, Spectra Physics) served as the source for two-photon excitation. All the measurements were taken for 60 s with a 63× Plan Apochromat oil immersion objective (N.A. = 1.4) (Zeiss, Germany). The excitation power measured at the objective ranged from 1.0 to 1.2 mW at 1000 nm. These power levels were sufficiently low to avoid saturation and bleaching (42). Both EGFP and mCherry can be simultaneously excited with 1000 nm two-photon excitation. The fluorescence emission was separated into two different detection channels with a 580 nm dichroic mirror (585DCXR, Chroma Technology, Rochingham, VT). The green channel was equipped with an 84 nm wide band-pass filter centered at 510 nm (FF01-510/84-25 Semrock, Rochester, NY) to eliminate the reflected fluorescence of mCherry.

Data analysis

Single channel brightness values were determined by a generalized form of Mandel's Q-parameter analysis with the brightness $\varepsilon_{segment}$ calculated for each second of photon count data (43,44). The average $\langle\varepsilon_{segment}\rangle$ represents the apparent brightness value of the sample. The normalized brightness b is calculated dividing the average brightness by the monomer GFP brightness that was independently measured at the beginning of the experiments, $b = \langle\varepsilon_{segment}\rangle/\varepsilon_{monomer}$. If the sample is a two species mixture, the apparent brightness is then given by a nonlinear combination of the brightness ε and the occupation number N of each species, $\langle\varepsilon_{segment}\rangle = (\varepsilon_1^2 N_1 + \varepsilon_2^2 N_2)/(\varepsilon_1 N_1 + \varepsilon_2 N_2)$ (45). The molar concentration of labeled proteins was determined from the intensity data according to (45). The scatter data were smoothed by binning into concentration intervals and calculation of the mean for each bin. Binning was accomplished by software written in Interactive Data Language. The algorithm requires a minimum of n data points per bin and a minimum bin interval of Δc. In case the interval Δc contains less than n data, the program dynamically increases the interval to ensure the minimum number of data points per bin is met. The mean of the binned data was plotted for each bin interval. The same procedure was also applied to brightness spike analysis, which has been described recently (39).

The same raw data were also used to calculate the autocorrelation function $g(\tau)$ (46). The experimental autocorrelation function $g(\tau)$ was fitted to theoretical functions using a two-dimensional (2D)-Gaussian beam profile to recover the residence or diffusion time τ_R. The residence time of monomeric and dimeric GFP have been characterized and scaled according to the Stokes-Einstein relation assuming spherical proteins (46). The residence time of functional proteins includes its interaction with cellular factors and is therefore not a direct measure of size (47). Nevertheless, the residence time reveals the mobility of the complex and can be used collaboratively with brightness analysis (39).

Spike count analysis was introduced to determine the relative concentration and apparent brightness of a rare but bright species that is mixed with a high concentration of a much dimmer species (39). A similar technique has been used to detect intensity spikes from an otherwise homogenous sample (48). A cut-off value of eight times the monomeric GFP brightness was used to select brightness spikes. The actual cut-off value was chosen to be high enough to differentiate the dim species (dimeric endophilins) from the bright species, but low enough to obtain sufficient brightness spikes within

the total length of the acquisition time. The data are segmented into intervals of 1 s, and the brightness $\varepsilon_{segment}$ is determined for each segment interval. The spike-count rate (SCR) in units of events per minute is defined by the number of events that have $\varepsilon_{segment}$ value greater than the cut-off value per 60 s of data. The maximal possible value is 60 min^{-1} for a segment interval of 1 s. Although choosing a shorter segment time increases this maximum number, the uncertainty in the brightness calculation increases as well and makes the identification of spikes more difficult.

Dual-color HSP analysis was performed as previously described (38,39). HSP identifies the heterospecies, which consists of GFP- and GFP-mCherry-labeled protein species. Complexes that carry only the mCherry label are excluded by the analysis. The HSP-brightness vector $\mathbf{b} = (b_r, b_g)$ identifies the heterospecies with b_g and b_r representing the brightness observed in the green and red detection channel, respectively. Each HSP-brightness corresponds to a point on a 2D brightness plot. If the heterospecies values consist of only the green species, then the b_g and b_r ratio will follow the GFP intensity ratio of the two channels, and the **b** vector will fall along the "green species only line." If the heterospecies values consist of a green- and red-labeled species, then the b_g and b_r ratio will deviate from the GFP intensity ratio, and the **b** vector will fall in the "green-red comobile zone." Each day that measurements were taken, GFP and a GFP-mCherry fusion protein were used as calibration markers for the green-only and green-red species, respectively.

RESULTS

Association of EndoB1 with cytoplasmic vesicles

Brightness analysis (49) was used to compare the oligomeric states of GFP-tagged EndoA2 and EndoB1 in the cytoplasm of U2OS cells. As stated, we previously reported that EndoA2, and the closely related isoform EndoA1, exist almost exclusively as tight homodimers in the cytoplasm of CV-1 cells (35). In contrast, a plot of normalized brightness units as a function of EndoB1-GFP concentration shows that EndoB1 can associate into higher order complexes (Fig. 1, *A* and *B*). The normalized brightness units were very scattered, and the degree of scatter was not reduced by simply increasing the number of experiments. Although the lowest brightness units obtained were ~2, indicative of dimers, brightness units of ~5–10 clearly predominated. To ascertain that this difference between EndoB1 and EndoA2 was not the result of differences between cell lines, we characterized the brightness of EndoA2 in U2OS cells and found that, as in CV-1 cells, a dimeric brightness value was retained throughout the concentration range examined (Fig. 1 *A*).

The fluorescence intensity trace taken from U2OS cells expressing EndoB1-GFP is mainly constant (Fig. S1 *A* in the Supporting Material). Unlike the intensity, brightness is a sensitive marker of rare but intense fluctuations. A graph of the brightness $\varepsilon_{segment}$ determined every second along the data trace resulted in numerous brightness spikes (Fig. S1 *B*) when the individual data traces of EndoB1 were subjected to $\varepsilon_{segment}$ analysis, indicating that rare but bright species were intermixed with dim species of EndoB1. Thus, the scatter in the average brightness values of EndoB1 in Fig. 1 *A* most likely reflects the statistical variations in the detection of rare but bright events during an FFS measurement. To better visualize the data trend we reduced the scatter by graphing the mean of the binned data ($n = 6$, $\Delta c = 200$ nM) in Fig. 1 *B*. As expected, EndoA2 has a brightness value of two across its concentration range, as the oligomerization of this protein is concentration independent. The average brightness of EndoB1 increases as a function of its average cellular concentration up to ~1 μM, and appears to plateau. This behavior suggests that the incorporation of EndoB1 into complexes may be saturating or subject to control by limiting cellular cofactors. Variation in the concentration of these putative cofactors from cell to cell could potentially also contribute to the observed scatter in EndoB1 brightness values.

We next turned to autocorrelation analysis to characterize the mobility of EndoB1 in cells. Single residence times, τ_{D1}, were obtained whenever autocorrelation curves could be described by single-species models. Otherwise, two species models were used to fit the curves and both τ_{D1} and τ_{D2} were obtained (Fig. S2). Among 58 cells examined, autocorrelation curves from 51 cells required two species fitting. A histogram of the residence times τ_{D1} and τ_{D2} for the 58 cells is

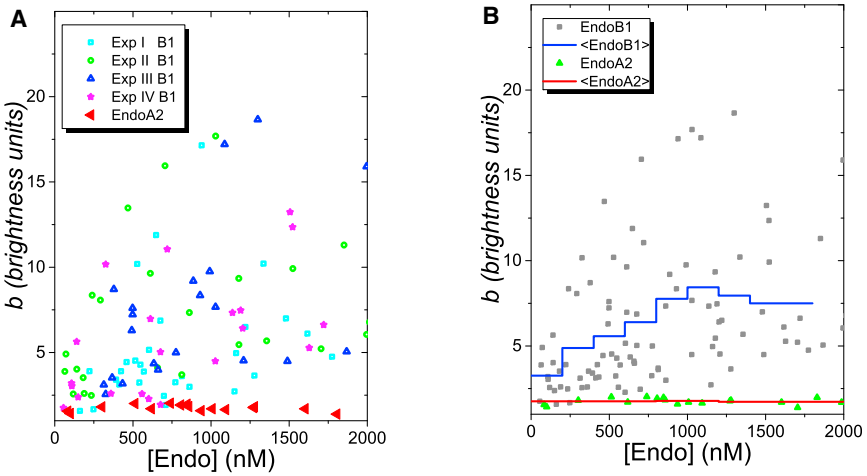

FIGURE 1 Brightness of EndoB1-GFP and EndoA2-GFP in U2OS cells. (*A*) Brightness titration experiments of EndoB1 and EndoA2. The normalized brightness is plotted versus the total labeled protein concentration. Four independent experiments with EndoB1 are displayed to illustrate reproducibility. Each symbol represents the measured normalized brightness from a different cell. The normalized brightness corresponds to the average protein copy number per diffusing complex. (*B*) The graph represents the mean of the binned data from (*A*) with $n = 6$ and $\Delta c = 200$ nM. To see this figure in color, go online.

displayed in Fig. 2 *A*. The average residence time τ_{D1} was 2.7 ms with a relative standard uncertainty of 55%, whereas the average residence time τ_{D2} was 58.5 ms with a relative standard uncertainty of 65%. For comparison, we also plotted the histogram of the residence times of EndoA2 (Fig. 2 *B*). In this case, virtually all the data could be described by a single-species model, yielding an average residence time of 2.54 ms with a relative standard uncertainty of 21%. Thus, the autocorrelation data corresponded well with the molecular brightness data and further support our original observation that EndoA2 exists largely as a soluble protein in the cytosol. In contrast, two distinct populations of EndoB1 coexist in the cytoplasm, one population consisting of small soluble species and the other having a much larger size and a higher EndoB1 copy number. Based on their brightness values and residence times, the larger particles likely represent a population of cytoplasmic membrane-bounded vesicles containing multiple copies of EndoB1.

The autocorrelation analysis suggests that a cytoplasmic and a vesicle-bound population of EndoB1 contribute to the measured brightness b of Fig. 1. The brightness of such a mixture is given by $b = f_1 b_1 + f_2 b_2$ with b_1 and b_2 representing the brightness of the cytoplasmic and vesicle-bound population. The fractional intensity f_1 is the ratio of the intensity from the cytoplasmic population to the total fluorescence intensity, whereas $f_2 = 1 - f_1$ is the fractional intensity of the vesicle-associated population. We use subscripts 1 and 2 to denote the cytoplasmic and vesicle-associated population throughout the rest of the work. We gain additional insight into the two terms $f_1 b_1 + f_2 b_2$ that determine the brightness of the mixture by considering the amplitudes a_1 and a_2 of the two-species fit to the autocorrelation function, since a_1/a_2 equals the ratio of the two brightness terms, $f_1 b_1/(f_2 b_2)$. The experimental amplitude ratio a_1/a_2 decreases with increasing brightness and levels off at large brightness values (Fig. S3). This result implies that the vesicle bound-population is mainly responsible for the observed brightness increase with concentration (Fig. 1 *B*).

The individual brightness values of the two species remain unresolved. However, because vesicles can contain several copies of the EndoB1, we expect that the brightness b_1 of the cytosolic species will be small when compared to the brightness b_2 of the vesicle-associated species. This is consistent with the observation of brightness spikes in Fig. S1 *B*, which reflect the presence of bright but rare vesicles. In case no vesicle event occurs during a short segment, the brightness of the segment is expected to be low and characterizes the dim, cytosolic species. Thus, a strategy for estimating the cytosolic brightness is to identify the lowest segmented brightness values of each experiment. The lowest values for the data in Fig. S1 *B* fall between a monomer and a dimer brightness. The same result was observed for 72% of the FFS measurements on EndoB1. Examples of such segmented brightness curves are shown in Fig. S4 for the measured concentration range. Because any labeled vesicles passing through part of the observation volume will raise the brightness of the segment, the minimum brightness value provides an upper bound for b_1. The brightness gain with concentration (Fig. 1 *B*) indicates that the number of bright vesicle events increases with concentration. Thus, it is expected to be more difficult to find segmented brightness values that are free of vesicle events at high than at low concentrations, which agrees with our observations. Over 90% of the FFS measurements at concentrations below 600 nM exhibit a minimum segmented brightness in the range of a monomer or dimer, while the percentage falls to 50% for $c > 1200$ nM. However, because we were able to find segmented brightness values that range from ~1 to ~2 over the entire concentration range, the data strongly suggest

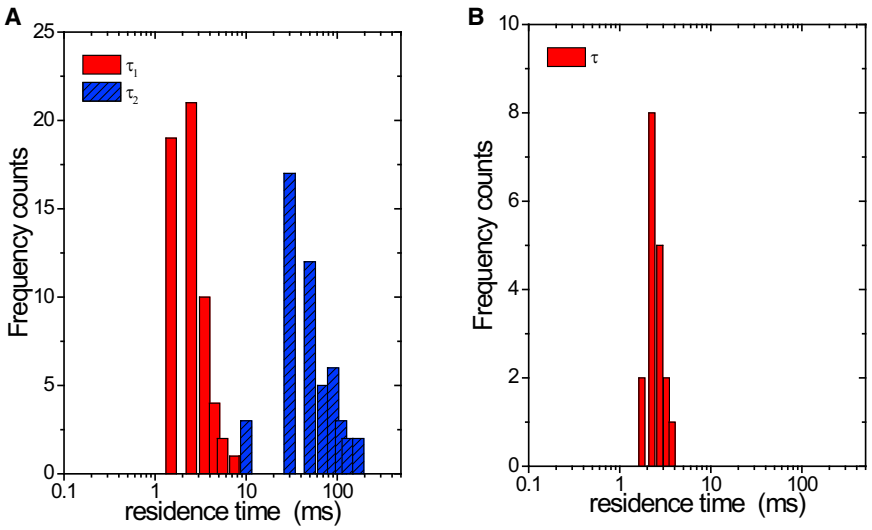

FIGURE 2 Distribution of residence times, τ_{D1} and τ_{D2}, recovered from the autocorrelation analysis of EndoB1 (*A*) and EndoA2 (*B*). For EndoB1, 51 cells from a total of 58 cells examined required a two species fit. The average residence time of the first species was 2.7 ± 1.5 ms and the average residence time of the second species was 58.5 ± 38.1 ms. For EndoA2, all the autocorrelations were fitted with a single species model with an average residence time of 2.5 ± 0.5 ms. To see this figure in color, go online.

that the oligomerization state of cytoplasmic EndoB1 cannot exceed a dimer.

Dyn2 promotes the formation of EndoB1-containing cytoplasmic vesicles

Dyn2 catalyzes membrane scission during the formation of endocytic vesicles from the plasma membrane and of transport vesicles from a subset of intracellular organelles, including the *trans*-Golgi network and late endosomes (reviewed in (50)). It was previously reported that, unlike A-type endophilins, EndoB1 does not contribute to the formation of endocytic vesicles from the plasma membrane (22). Therefore, we asked whether Dyn2 affected the generation of EndoB1-containing vesicles, which are likely to originate from intracellular organelles. To address this question, single species analysis was performed on cells that were cotransfected with EndoB1-GFP and Dyn2-mCherry. Only the brightness of EndoB1-GFP was measured and analyzed. Because the red fluorescence emission is completely outside of the green detection band, the presence of red fluorescent protein was ignored spectroscopically and was used solely to identify cells coexpressing both proteins. Fig. 3 displays the mean-binned ($n = 6$, $\Delta c = 200$ nM) brightness $\langle b \rangle$ of EndoB1 in the presence of exogenous Dyn2. At concentrations of EndoB1-GFP below 1 μM, coexpression of Dyn2 did not appreciably affect the brightness distribution (compared with Fig. 1 *A*). However, at higher EndoB1 concentrations, the brightness of EndoB1 in cells coexpressing exogenous Dyn2 did not saturate, as they had in cells expressing only endogenous Dyn2 (Fig. 1 *B*). Thus, it appears that Dyn2 is an important factor in the formation of EndoB1-containing vesicles. Similar experiments were performed with a dominant-negative Dyn2 mutant, K44A, which is known to interfere with membrane vesiculation in cells (51). The mean-binned ($n = 6$, $\Delta c = 200$ nM) brightness $\langle b \rangle$ of EndoB1 in cells coexpressing Dyn2(K44A) (Fig. 3) were clearly lower than in cells expressing either wild-type Dyn2 or only endogenous Dyn2 (see Fig. 1 *B*).

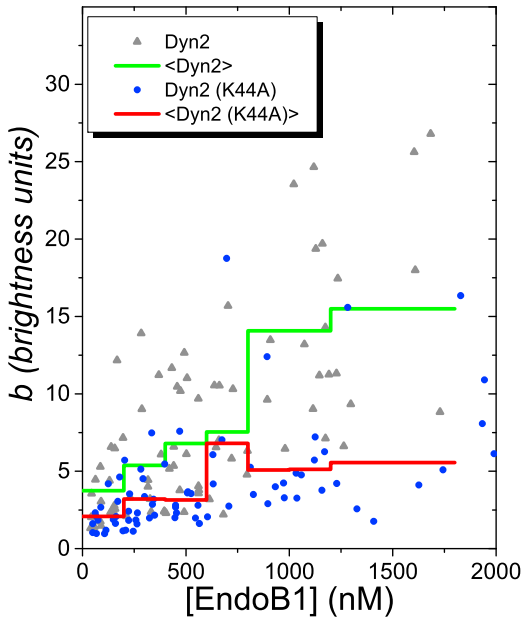

FIGURE 3 Brightness of EndoB1-GFP in the presence of exogenous Dyn2-mCherry (*gray solid triangles*) and Dyn2(K44A)-mCherry (*blue solid circles*). The green and red line represent the mean-binned ($n = 6$, $\Delta c = 200$ nM) brightness in the presence of Dyn2-mCherry and Dyn2(K44A)-mCherry, respectively. To see this figure in color, go online.

This difference could be explained by a higher concentration of EndoB1-containing vesicles with Dyn2 expression than with Dyn2(K44A) expression. However, it is also possible that the vesicle concentration is largely unchanged, but Dyn2 expression leads to brighter vesicles than does Dyn2(K44A) expression. The average brightness of the sample cannot distinguish between these two scenarios. We applied brightness spike analysis on the data presented in Fig. 3 to determine if exogenous Dyn2 affects the relative concentration of EndoB1-containing vesicles. As described in more detail in the Materials and Methods section, the brightness is calculated for every second of data acquisition. Bright but rare events give rise to brightness spikes on top of the background brightness of the dim species (Fig. S1 *B*). The SCR is determined by counting the number of spike events above a threshold value per minute of data acquisition time. The SCR is related to the concentration of bright species (39), which, in this case, are EndoB1-enriched complexes. A SCR of 0 min^{-1} corresponds to the absence of brightness spikes in the sample. The SCR value increases as the concentration of the bright species increases and saturates at 60 min^{-1}, which is caused by a brightness above the threshold value during every second of collected data.

The SCR values in the presence of exogenous Dyn2 and Dyn2(K44A) are graphed as a function of labeled EndoB1 concentration (Fig. 4). Although the individual SCR values are scattered, it appears that Dyn2 generally leads to higher SCR values than the dominant-negative Dyn2. We binned the data ($n = 6$, $\Delta c = 200$ nM) to reduce the scatter. As expected the mean-binned SCR curve with Dyn2 exceeds the mean-binned SCR curve with Dyn2(K44A) (Fig. 4). Thus, at any given concentration of labeled EndoB1 the number of observed brightness spikes is higher with Dyn2 than with Dyn2(K44A). A higher SCR indicates a higher concentration of EndoB1-containing vesicles, which provides an explanation for the brightness increase observed in Fig. 3. We also calculated the SCR of the EndoB1 data shown in Fig. 1 (Fig. S5) and plotted the mean-binned ($n = 6$, $\Delta c = 200$ nM) SCR in Fig. 4. These data reflect the SCR for cells in the presence of endogenous Dyn2. Interestingly, the averaged brightness spike rate for endogenous SCR falls in between the rates observed for exogenously expressed Dyn2 and the dominant-negative Dyn2 mutant, K44A. In addition, the averaged brightness of EndoB1 in cells

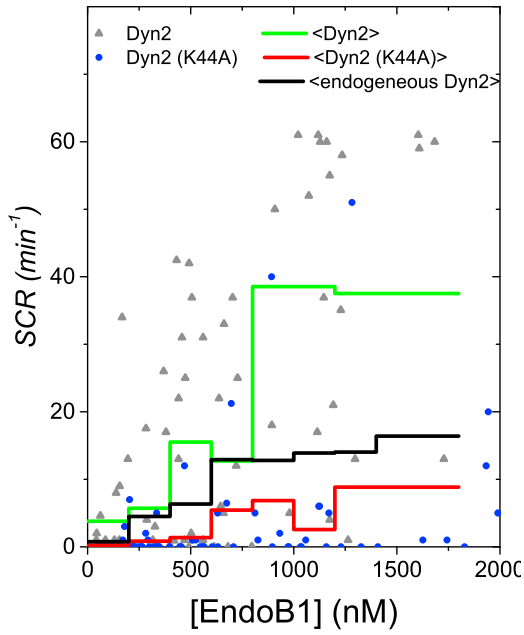

FIGURE 4 SCR of EndoB1 versus the labeled EndoB1 concentration. The green line represents the mean ($n = 6$, $\Delta c = 200$ nM) of the binned spike count rate for EndoB1-GFP in the presence of Dyn2-mCherry. The red line corresponds to the mean ($n = 6$, $\Delta c = 200$ nM) of the binned spike count rate for EndoB1-GFP in the presence of Dyn2(K44A)-mCherry. To see this figure in color, go online.

coexpressing Dyn2(K44A) (Fig. 3) were clearly lower than in cells expressing only endogenous Dyn2 (Fig. 1 *B*). Taken together, these results indicate that active Dyn2 acts as a cofactor to promote the formation of EndoB1-containing vesicles.

CAV1 associates with EndoB1-containing vesicles

Having established that EndoB1 is associated with vesicles, we sought to further characterize these vesicles by identifying their coat proteins. We used HSP analysis to determine whether EndoB1-GFP comigrates with either CAV1-mCherry or clathrin light chain (CLC)-mCherry. HSP allows detection and quantification of the coexistence of two species within the same complex (38). As described in Materials and Methods, each HSP-brightness vector $\mathbf{b} = (b_R, b_G)$ identifies a point on a 2D brightness plot (Fig. 5 *A*). HSP-values that fall on the green line of that plot denote a green-labeled species that does not interact with the red-labeled protein. Any association of red-labeled protein with the green-labeled protein displaces the HSP brightness away from the green line into the gray area, which we call the green-red comobile zone. Brightness vectors that fall along a line within the green-red comobile zone have the same ratio of green- and red-labeled proteins per complex (*dashed lines*, Fig. 5 *A*). A larger slope of the line corresponds to a higher ratio of the green- to red-label. Thus, at a given green value, a species with a higher red brightness value b_r contains more red proteins than a species with a lower b_r value (e.g., sample II and sample I in Fig. 5 *A*).

We first determined whether we could detect the comigration of CLC-mCherry with GFP-tagged epsin1, a protein known to play an important role in clathrin-mediated endocytosis (52). As shown in Fig. 5 *B*, virtually all the HSP vectors were in the green-red comobile zone, demonstrating that epsin1 was indeed associated with clathrin-coated vesicles. In contrast, when cells coexpressing GFP-epsin1 with CAV1-mCherry were examined, the HSP brightness vectors were largely distributed along the green line (Fig. 5 *B*). Moreover, the relatively few data points that distributed to the green-red co-mobile zone had much lower b_r values than those obtained with the GFP-epsin1/CLC-mCherry system. Thus, our results indicate that epsin1 associates preferentially with clathrin-coated rather than caveolin-coated vesicles.

We then tested whether EndoB1 associates with vesicles containing clathrin or caveolin. Fig. 6 shows that all HSP vectors from cells expressing EndoB1-GFP and CLC-mCherry localized along the green species only line, whereas many of the HSP vectors from cells expressing EndoB1-GFP and CAV1-mCherry were found in the green-red comobile zone, confirming the association of EndoB1 with caveolin-containing vesicles. In contrast, HSP was unable to detect association between EndoB1 and clathrin-containing vesicles. This negative result could potentially arise from the absence of clathrin-containing vesicles in the sample, which cannot be ruled out by HSP. However, brightness spikes in the red-detection channel clearly indicate the presence of mCherry-labeled clathrin-containing vesicles (Fig. S7). If these clathrin-containing vesicles exist at a much lower concentration than the EndoB1-containing vesicles, then HSP analysis would be dominated by the brightness of the EndoB1-GFP carrying vesicles, and therefore we would be unable to identify the interaction. Although the concentration of the vesicles cannot be directly quantified, the segmented brightness provides additional insight. A strong association of EndoB1-GFP with CLC-mCherry should result in simultaneous brightness spikes in the green- and red-detection channel to indicate the presence of both proteins on a vesicle. However, brightness spikes in both channels appeared uncorrelated as illustrated in Fig. S7. These observations suggest that the association of EndoB1 with clathrin-containing vesicles, if it exists, is either weak or only involves a small subset of the vesicles.

Ligand-dependent association of EGFR and EndoB1-containing cytoplasmic vesicles

EGFR is known to migrate through the cytoplasm on both clathrin-coated (53) and caveolin-coated (54) vesicles. We employed HSP analysis to determine if a subset of the EndoB1-containing particles could represent cytoplasmic

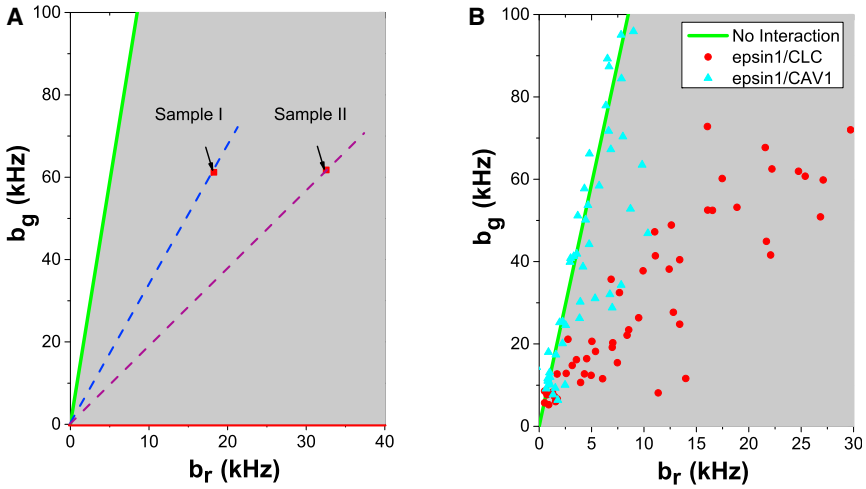

FIGURE 5 HSP analysis of cells cotransfected with green and red fluorescent-labeled proteins. (*A*) Dual-color HSP brightness plot: The gray shaded zone represents all possible brightness values that identify the presence of protein complexes carrying both green and red labels. Samples I and II have the same average amount of green-labeled proteins per diffusing complex, but sample II contains more red-labeled proteins per diffusing complex than sample I. The green line represents the limit where complexes carrying both colors are absent. (*B*) The HSP brightness values for GFP-Epsin1 and CLC-mCherry (*red solid circles*) and for GFP-Epsin1 and CAV1-mCherry (*blue solid triangles*). To see this figure in color, go online.

transport vesicles that deliver EGFR from one organelle to another in these pathways. The resulting HSP brightness vectors were analyzed and plotted in Fig. 7 *A*. Under normal growth conditions, most HSP brightness vectors were in the green-red comobile zone, demonstrating that EndoB1 associates with a subset of vesicles that also contain EGFR. If EndoB1 is a genuine factor for transporting EGFR, we would also expect that the association of EGFR and EndoB1 will respond to EGF. Indeed, the HSP brightness vectors clustered around a low-brightness region upon serum starvation, which is consistent with a reduction in the number of EGFR-containing vesicles. Upon adding 100 ng/ml EGF, the HSP brightness values increased, indicating that EndoB1 is able to associate with ligand-activated EGFR vesicles (Fig. 7 *B*).

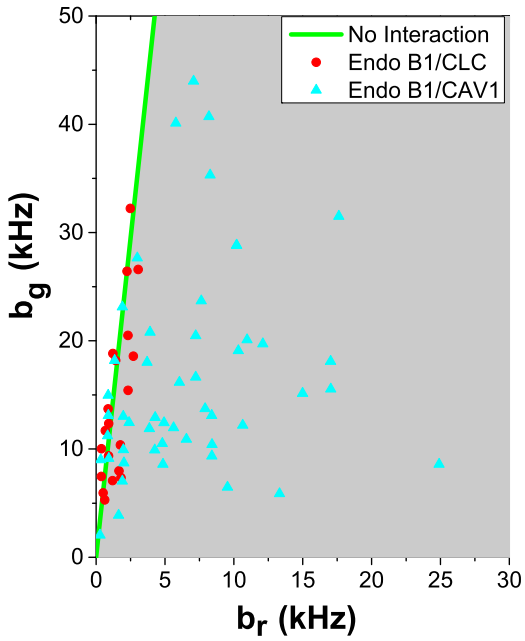

FIGURE 6 HSP analysis of EndoB1. The HSP brightness values for EndoB1-GFP and CLC-mCherry (*red solid circles*) and for EndoB1-GFP and CAV1-mCherry (*blue solid triangles*). To see this figure in color, go online.

It has been reported that clathrin-mediated endocytosis of EGFRs is induced by low EGF concentrations (e.g., 1.5 ng/ml; equivalent to the endogenous EGF concentration present in serum), whereas caveolin-mediated EGFR uptake predominates at EGF concentrations higher than ~20 ng/ml ((54), but see (55) for a conflicting view). To determine if EndoB1 and EGFR associate with each other under conditions that favor EGFR transport on clathrin-coated vesicles, HSP brightness vectors were obtained using serum-starved cells or cells treated with 1.5 ng/ml EGF (Fig. S6).The slope of the brightness vectors were similar in both cases, although a higher fraction of brightness values were located in the low-brightness region upon serum starvation. We plotted the HSP brightness versus the intensity of each channel together with the mean of the binned data ($n = 5$, DF = 30 kcps) to investigate this difference (Fig. 8, *A* and *B*). The green HSP brightness b_g was greater in EGF-treated cells than in serum-starved cells at every intensity F_g of the green channel (Fig. 8 *A*). Because F_g is proportional to the concentration of EGFR-EGFP, this result indicates that EGF treatment increases the brightness of EGFR-EGFP at every concentration of labeled receptor. Similarly, the red HSP brightness b_r increased for every intensity F_r of the red channel (Fig. 8 *B*). Taken together, these data suggest that adding EGF at 1.5 ng/ml produced an increase in the brightness of EGFR-EGFP and EndoB1-mCherry, which is consistent with the presence of a higher concentration of vesicles carrying both proteins. Thus, it appears that EndoB1 is associated with EGFR in vesicles mobilized by the addition of EGF at a concentration known to induce only clathrin-mediated endocytosis. Finally, we performed spike count analysis of the data from the green channel. The SCR and the mean-binned SCR ($n = 5$, DF = 30 kcps) demonstrate an increase in the number of bright events in the green channel

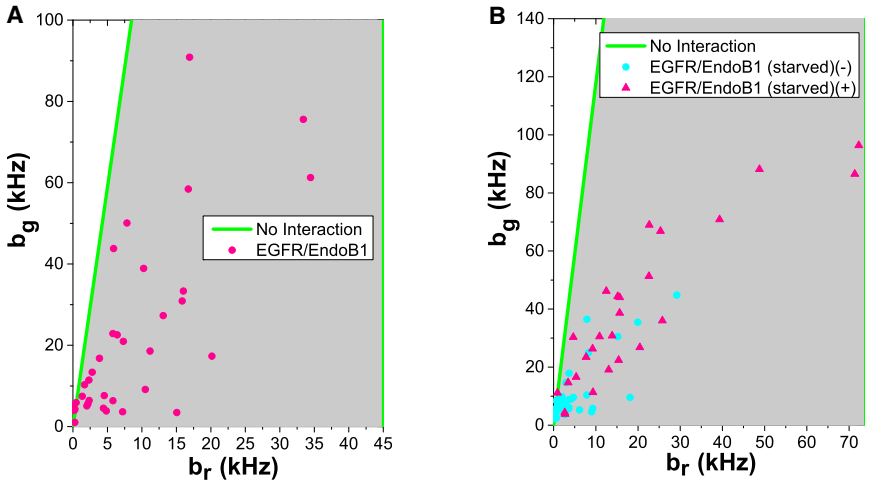

FIGURE 7 HSP analysis of EGFR and EndoB1. (*A*) HSP brightness values for EGFR-EGFP and EndoB1-mCherry under normal growth condition. (*B*) HSP brightness values for EGFR-EGFP and EndoB1-mCherry when serum starved for at least 4 h (*red solid circles*) and after incubation with EGF (100 ng/ml) for 0.5 h (*blue solid triangles*). To see this figure in color, go online.

upon adding the ligand (Fig. 8 *C*). This establishes that the number of EGFR-containing vesicles increased by addition of EGF.

DISCUSSION

Our studies highlight the use of FFS for characterizing small cytoplasmic complexes, such as interorganelle transport vesicles, which are below the limit of resolution of conventional live-cell imaging approaches. In contrast to the early stages of endocytosis on the plasma membrane, which have been studied effectively using total internal reflection fluorescence microscopy, few biophysical techniques are available to directly examine the trafficking of intracellular vesicles. Three-dimensional single-particle tracking approaches have provided insight into the trajectories, spatial confinement, and energy dependence of moving vesicles, but have been less informative regarding their protein composition. FFS is ideally suited to study the protein composition of intracellular vesicles. Intracellular vesicles are typically present at low concentrations, but each vesicle has multiple copies of a particular protein, giving rise to large fluctuations easily detected by FFS measurements. In this study, we showed that multiple copies of EndoB1 associate with vesicles that also contain multiple copies of caveolin, but which are largely devoid of clathrin. These results also highlight the specificity of the vesicle formation process, because EndoB1 and clathrin were not observed on the same vesicle even under cooverexpression conditions (Fig. 5).

Both autocorrelation and brightness analyses reveal that EndoB1 exists as multiple species (Figs. S1 *B* and 2). Autocorrelation identifies a fast and a slow diffusing species. The fast diffusing species has an average residence time of

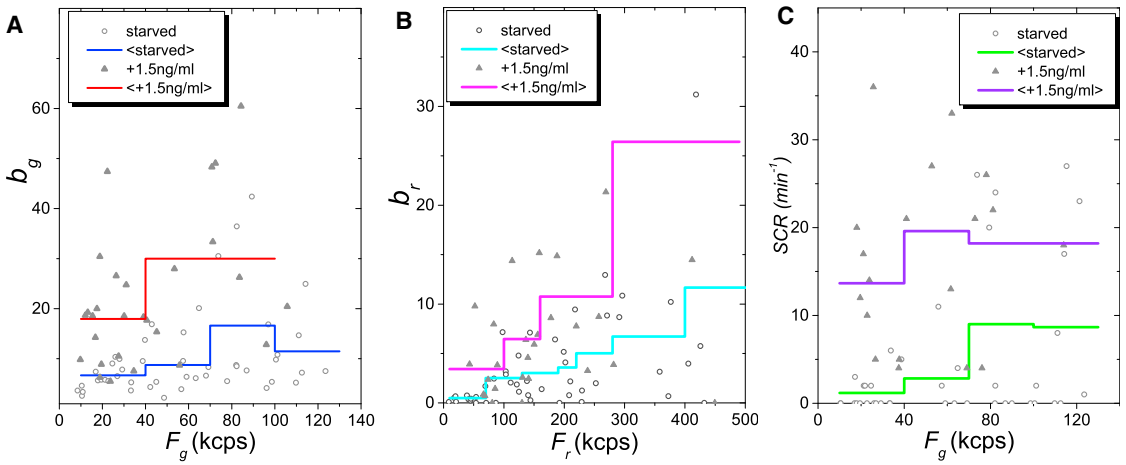

FIGURE 8 HSP brightness for EGFR-EGFP and EndoB1-mCherry versus intensity when serum starved for at least 4 h (*blue solid circles*) and after incubation with EGF (1.5 ng/ml) for 0.5 h (*red solid triangles*). (*A*) Green-channel brightness b_g versus green-channel intensity F_g and mean-binned data. (*B*) Red-channel brightness b_r versus red-channel intensity F_r and mean-binned data. (*C*) Spike count rate of the green channel versus F_g and mean-binned data. To see this figure in color, go online.

~2.5 ms, similar to that of EndoA2 and corresponding to the residence time of a soluble protein in the cytoplasm. The slowly diffusing species has an average residence time close to 60 ms, consistent with its association with cytoplasmic vesicles. The brightness spikes (Fig. S1 *B*) reveal that the second species consists of rare but bright particles. The low number of events of the rare species introduces considerable scatter into the measured FFS parameters.

It is currently not feasible to quantify the brightness and concentration fraction of each species. First, the concentration fraction for the individual species cannot be determined from autocorrelation analysis alone, because the brightness associated with each diffusing species is unknown. Second, the signal/noise ratio of FFS experiments in cells is generally not sufficient to identify the brightness of each species in a mixture (56). Although combining autocorrelation and brightness analysis could facilitate resolution of a binary mixture in certain circumstances, this approach is not suitable for our study. First, the small number of bright events already introduces significant scatter in the average brightness measured in each cell (Fig. 1 *A*). A meaningful separation of brightness or concentration into two species appears futile under these conditions. Second, it is likely that the copy number of EndoB1 varies from vesicle to vesicle, which would lead to a distribution of brightness species, complicating quantitative modeling efforts.

We sought to gain insight into the nature of the EndoB1 complexes by considering the average brightness, which for a mixture of two species with normalized brightness b_i and fractional intensity f_i for species i is $b = f_1 b_1 + f_2 b_2$. We noticed that for the majority of data sets the lowest brightness in a one-second segment was between a monomer and a dimer (Figs. S1 *B* and S4). As explained earlier we expect that these segments represent the properties of the soluble fraction with minimal or no interference from vesicle-bound EndoB1. We therefore concluded that the oligomeric state of soluble EndoB1 is not higher than a dimer over the entire concentration range studied. Because the cytoplasmic brightness b_1 is limited to not exceed two and the fractional intensity f_1 has to be ≤ 1, the maximum contribution from the cytoplasmic population to the brightness is $f_1 b_1 = 2$. Thus, the increase in brightness above two in Fig. 1 *B* is due to vesicle-bound EndoB1. This conclusion is further corroborated by the behavior of the amplitude ratio a_1/a_2, which equals $f_1 b_1 / f_2 b_2$. This ratio decreased as b increased (Fig. S3), which demonstrates that the vesicle-bound contribution $f_2 b_2$ to the total brightness b grows relative to the cytoplasmic component $f_1 b_1$. Thus, the increase in the brightness b predominantly reflects an increase in the copy number or concentration fraction of vesicle-bound EndoB1. Spike count analysis enables us to identify if the increase in average brightness mainly reflects a growth in the relative vesicle concentration or in the protein copy number per vesicle. Using this approach we demonstrated that Dyn2(K44A) decreased the population of labeled EndoB1-containing vesicles and that adding EGF to starved cells increased the population of EGFR vesicles.

The low number of bright vesicle events captured during each data acquisition interval introduced significant scatter in the measured brightness values (Fig. 1 *A*). Averaging of brightness measurements from cells expressing labeled EndoB1 at similar concentrations is expected to reduce the scatter, because the number of sampled vesicle events is increased. Indeed, the concentration dependence of the brightness data only became apparent after binning of the data in concentration intervals and determination of the mean brightness from each bin (Fig. 1 *B*). The brightness of EndoB1 increases with protein concentration until it plateaus at concentrations higher than 1 μM. We believe this saturation reflects a limiting cellular factor. One such factor implicated by our data is Dyn2, which may be present in limiting amount in cells. Upon overexpression of Dyn2, the brightness values of EndoB1 increased continuously as a function of EndoB1 concentration (Fig. 3). Overexpression of a dominant-negative Dyn2 mutant resulted in a significant reduction of brightness (Fig. 3). Thus, it appears that the activity of endogenous Dyn2 is sufficient to accommodate low concentrations of EndoB1. However, EndoB1 brightness saturates at higher EndoB1 concentrations because of the limiting activity of endogenous Dyn2.

The residence times of EndoB1-containing cytoplasmic particles, together with the involvement of Dyn2 in their formation, strongly suggests that they represent membrane-bounded transport vesicles. This possibility was further supported by our finding that EndoB1 comoves with an integral membrane protein, the EGFR, and by a very recent report showing that Dyn2 and EndoB1 cooperate in the formation of vesicles containing Atg9, an integral membrane component of the autophagic pathway (57). The EGFR is a classic marker of biosynthetic and endocytic membrane trafficking pathways. Newly synthesized EGFR transits through the endoplasmic reticulum and Golgi apparatus on its way to the plasma membrane (58). After EGF-dependent internalization, it then shuttles through multiple endocytic compartments that mediate its recycling or lysosomal degradation. In our studies, we typically monitored changes in the association of EGFR with EndoB1-containing particles 30 min after cells were treated with EGF. Thus, it is likely that these changes reflect events occurring at later stages of the endocytic process, and are not directly related to the formation of endocytic vesicles at the plasma membrane.

An early report claimed that the EGFR is internalized predominantly via clathrin-mediated endocytosis when cells are exposed to low (1.5 ng/ml) EGF concentrations, and additionally via clathrin-independent mechanisms when exposed to high (20 ng/ml and higher) EGF concentrations (54). Because high EGF concentrations induced sorting of EGFRs into caveolin-positive structures on the plasma membrane, it was surmised that caveolar uptake accounted

for a major portion of the clathrin-independent EGFR internalization. However, the importance of caveolin-mediated EGFR endocytosis has been questioned in several more recent reports (55,59) and new data point to a role for caveolin in EGFR trafficking in later stages of degradative endocytosis, such as transport from late endosomes to lysosomes (60). This finding is consistent with reports that EndoB1 also promotes late endocytic trafficking by acting in complex with Beclin and PI3KC3 (Vps34) (61). Therefore, we suspect that EndoB1 is associated with caveolin in the late stages of degradative endocytosis. Our data also indicate that the association between EndoB1 and caveolin is not 100%, as some of the HSP brightness vectors fell on the green species only line (Fig. 6), suggesting that caveolin may not be the sole coat protein involved in EndoB1-mediated transport. For example, we observed association of EndoB1 and EGFR in vesicles mobilized under conditions known to induce only clathrin-mediated endocytosis (Figs. S6 and 8). On the other hand, no apparent association of EndoB1 and CLC on vesicles was detected in this study (Figs. 6 and S7). It is not obvious how these two observations can be reconciled. It might be possible that EndoB1 only associates with EGFR after clathrin dissociated from the EGFR vesicles. Alternatively, EndoB1 may associate only with a small subset of clathrin-containing vesicles, which would lead to HSP data that appear close to the noninteracting line. Further work will be required to conclusively identify the transport processes mediated by EndoB1-containing vesicles and to clarify the mechanistic aspects underlying recruitment of EndoB1 to these vesicles.

The HSP brightness values for some samples seem strongly correlated with data points that appear to fall along a line, such as observed for epsin1 and CLC (Fig. 5 *B*) and for EGFR and EndoB1 (Fig. 7). Such a correlation suggests that the copy numbers of the two proteins associated with a vesicle are linked. This link might be caused by direct physical interactions as suggested by literature for epsin1 and CLC (62). However, it is also possible that such a link is established indirectly by intermediary factors. Our data suggest that the copy number of EGFR and EndoB1 are linked. A direct physical interaction between these two proteins has not been reported. However, EndoB1 has been demonstrated to be important for the degradative endocytic pathway for EGFR (31,61). Therefore, it is possible that the association of EGFR and EndoB1is mediated by some currently unknown factor.

Our study demonstrates that fluctuation spectroscopy can contribute to our understanding of intracellular trafficking events by providing insight into the association of proteins with small cytoplasmic vesicles in live cells. We showed that brightness and brightness spike analysis offers a promising approach to detect the influence of perturbations, such as added ligands, on the labeled vesicle population. This strategy allowed us to identify changes in the relative concentration of the fluorescent vesicle population. Fluctuation data from cellular vesicles are not trivial to analyze. We believe that the approaches described in this work provide a useful starting point for future work and will serve to stimulate the development of improved analytical procedures.

SUPPORTING MATERIAL

Seven figures are available at http://www.biophysj.org/biophysj/supplemental/S0006-3495(16)30463-5.

AUTHOR CONTRIBUTIONS

J.L. designed and performed experiments and analyzed data. J.P.A. and B.B. contributed to experimental design and writing of the article. J.P.E. designed experiments and contributed analysis tools. J.D.M. designed experiments and analyzed data. Y.C. designed experiments, analyzed data, and wrote the article.

ACKNOWLEDGMENTS

J.L., J.D.M., and Y.C. are supported by grants from the National Institutes of Health (GM64589 and GM091743). J.P.E. is supported by the National Institutes of Health (T32HL007741).

REFERENCES

1. Kjaerulff, O., L. Brodin, and A. Jung. 2011. The structure and function of endophilin proteins. *Cell Biochem. Biophys.* 60:137–154.
2. Farsad, K., N. Ringstad, …, P. De Camilli. 2001. Generation of high curvature membranes mediated by direct endophilin bilayer interactions. *J. Cell Biol.* 155:193–200.
3. Gallop, J. L., C. C. Jao, …, H. T. McMahon. 2006. Mechanism of endophilin N-BAR domain-mediated membrane curvature. *EMBO J.* 25:2898–2910.
4. Masuda, M., S. Takeda, …, N. Mochizuki. 2006. Endophilin BAR domain drives membrane curvature by two newly identified structure-based mechanisms. *EMBO J.* 25:2889–2897.
5. Weissenhorn, W. 2005. Crystal structure of the endophilin-A1 BAR domain. *J. Mol. Biol.* 351:653–661.
6. Cui, H., G. S. Ayton, and G. A. Voth. 2009. Membrane binding by the endophilin N-BAR domain. *Biophys. J.* 97:2746–2753.
7. Jao, C. C., B. G. Hegde, …, R. Langen. 2010. Roles of amphipathic helices and the bin/amphiphysin/rvs (BAR) domain of endophilin in membrane curvature generation. *J. Biol. Chem.* 285:20164–20170.
8. Suresh, S., and J. M. Edwardson. 2010. The endophilin N-BAR domain perturbs the structure of lipid bilayers. *Biochemistry.* 49:5766–5771.
9. Mim, C., H. Cui, …, V. M. Unger. 2012. Structural basis of membrane bending by the N-BAR protein endophilin. *Cell.* 149:137–145.
10. Dittman, J., and T. A. Ryan. 2009. Molecular circuitry of endocytosis at nerve terminals. *Annu. Rev. Cell Dev. Biol.* 25:133–160.
11. Ringstad, N., Y. Nemoto, and P. De Camilli. 1997. The SH3p4/Sh3p8/SH3p13 protein family: binding partners for synaptojanin and dynamin via a Grb2-like Src homology 3 domain. *Proc. Natl. Acad. Sci. USA.* 94:8569–8574.
12. de Heuvel, E., A. W. Bell, …, P. S. McPherson. 1997. Identification of the major synaptojanin-binding proteins in brain. *J. Biol. Chem.* 272:8710–8716.

13. Boucrot, E., A. Pick, …, M. M. Kozlov. 2012. Membrane fission is promoted by insertion of amphipathic helices and is restricted by crescent BAR domains. *Cell.* 149:124–136.
14. Gad, H., N. Ringstad, …, L. Brodin. 2000. Fission and uncoating of synaptic clathrin-coated vesicles are perturbed by disruption of interactions with the SH3 domain of endophilin. *Neuron.* 27:301–312.
15. Schuske, K. R., J. E. Richmond, …, E. M. Jorgensen. 2003. Endophilin is required for synaptic vesicle endocytosis by localizing synaptojanin. *Neuron.* 40:749–762.
16. Sundborger, A., C. Soderblom, …, O. Shupliakov. 2011. An endophilin-dynamin complex promotes budding of clathrin-coated vesicles during synaptic vesicle recycling. *J. Cell Sci.* 124:133–143.
17. Verstreken, P., O. Kjaerulff, …, H. J. Bellen. 2002. Endophilin mutations block clathrin-mediated endocytosis but not neurotransmitter release. *Cell.* 109:101–112.
18. Milosevic, I., S. Giovedi, …, P. De Camilli. 2011. Recruitment of endophilin to clathrin-coated pit necks is required for efficient vesicle uncoating after fission. *Neuron.* 72:587–601.
19. Dong, Y., Y. Gou, …, J. Bai. 2015. Synaptojanin cooperates in vivo with endophilin through an unexpected mechanism. *eLife.* 4:e05660.
20. Renard, H.-F., M. Simunovic, …, L. Johannes. 2015. Endophilin-A2 functions in membrane scission in clathrin-independent endocytosis. *Nature.* 517:493–496.
21. Boucrot, E., A. P. A. Ferreira, …, H. T. McMahon. 2015. Endophilin marks and controls a clathrin-independent endocytic pathway. *Nature.* 517:460–465.
22. Modregger, J., A. A. Schmidt, …, M. Plomann. 2003. Characterization of Endophilin B1b, a brain-specific membrane-associated lysophosphatidic acid acyl transferase with properties distinct from endophilin A1. *J. Biol. Chem.* 278:4160–4167.
23. Cuddeback, S. M., H. Yamaguchi, …, H.-G. Wang. 2001. Molecular cloning and characterization of Bif-1. A novel Src homology 3 domain-containing protein that associates with Bax. *J. Biol. Chem.* 276:20559–20565.
24. Pierrat, B., M. Simonen, …, J. Heim. 2001. SH3GLB, a new endophilin-related protein family featuring an SH3 domain. *Genomics.* 71:222–234.
25. Zhang, C., A. Li, …, H. Xiao. 2011. A novel TIP30 protein complex regulates EGF receptor signaling and endocytic degradation. *J. Biol. Chem.* 286:9373–9381.
26. Rostovtseva, T. K., H. Boukari, …, R. J. Youle. 2009. Bax activates endophilin B1 oligomerization and lipid membrane vesiculation. *J. Biol. Chem.* 284:34390–34399.
27. Etxebarria, A., O. Terrones, …, G. Basañez. 2009. Endophilin B1/Bif-1 stimulates BAX activation independently from its capacity to produce large scale membrane morphological rearrangements. *J. Biol. Chem.* 284:4200–4212.
28. Karbowski, M., S.-Y. Jeong, and R. J. Youle. 2004. Endophilin B1 is required for the maintenance of mitochondrial morphology. *J. Cell Biol.* 166:1027–1039.
29. Takahashi, Y., C. L. Meyerkord, and H.-G. Wang. 2008. BARgaining membranes for autophagosome formation: regulation of autophagy and tumorigenesis by Bif-1/Endophilin B1. *Autophagy.* 4:121–124.
30. Stenmark, H. 2010. The Sir Hans Krebs Lecture. How a lipid mediates tumour suppression. Delivered on 29 June 2010 at the 35th FEBS Congress in Gothenburg, Sweden. *FEBS J.* 277:4837–4848.
31. Runkle, K. B., C. L. Meyerkord, …, H.-G. Wang. 2012. Bif-1 suppresses breast cancer cell migration by promoting EGFR endocytic degradation. *Cancer Biol. Ther.* 13:956–966.
32. Wong, A. S. L., R. H. K. Lee, …, N. Y. Ip. 2011. Cdk5-mediated phosphorylation of endophilin B1 is required for induced autophagy in models of Parkinson's disease. *Nat. Cell Biol.* 13:568–579.
33. Takahashi, Y., C. L. Meyerkord, …, H.-G. Wang. 2011. Bif-1 regulates Atg9 trafficking by mediating the fission of Golgi membranes during autophagy. *Autophagy.* 7:61–73.
34. Wang, D. B., T. Uo, …, R. S. Morrison. 2014. Bax interacting factor-1 promotes survival and mitochondrial elongation in neurons. *J. Neurosci.* 34:2674–2683.
35. Ross, J. A., Y. Chen, …, D. M. Jameson. 2011. Dimeric endophilin A2 stimulates assembly and GTPase activity of dynamin 2. *Biophys. J.* 100:729–737.
36. Elson, E. L. 2013. 40 years of FCS: how it all began. *Methods Enzymol.* 518:1–10.
37. Chen, Y., J. Johnson, …, J. D. Mueller. 2010. Observing protein interactions and their stoichiometry in living cells by brightness analysis of fluorescence fluctuation experiments. *Methods Enzymol.* 472:345–363.
38. Wu, B., Y. Chen, and J. D. Müller. 2010. Heterospecies partition analysis reveals binding curve and stoichiometry of protein interactions in living cells. *Proc. Natl. Acad. Sci. USA.* 107:4117–4122.
39. Li, J., B. Barylko, …, Y. Chen. 2012. Molecular brightness analysis reveals phosphatidylinositol 4-Kinase IIβ association with clathrin-coated vesicles in living cells. *Biophys. J.* 103:1657–1665.
40. Carter, R. E., and A. Sorkin. 1998. Endocytosis of functional epidermal growth factor receptor-green fluorescent protein chimera. *J. Biol. Chem.* 273:35000–35007.
41. Wu, B., Y. Chen, and J. D. Müller. 2009. Fluorescence fluctuation spectroscopy of mCherry in living cells. *Biophys. J.* 96:2391–2404.
42. Hur, K.-H., P. J. Macdonald, …, J. D. Mueller. 2014. Quantitative measurement of brightness from living cells in the presence of photodepletion. *PLoS One.* 9:e97440.
43. Chen, Y., J. D. Müller, …, E. Gratton. 2002. Molecular brightness characterization of EGFP in vivo by fluorescence fluctuation spectroscopy. *Biophys. J.* 82:133–144.
44. Sanchez-Andres, A., Y. Chen, and J. D. Müller. 2005. Molecular brightness determined from a generalized form of Mandel's Q-parameter. *Biophys. J.* 89:3531–3547.
45. Chen, Y., L.-N. Wei, and J. D. Müller. 2003. Probing protein oligomerization in living cells with fluorescence fluctuation spectroscopy. *Proc. Natl. Acad. Sci. USA.* 100:15492–15497.
46. Thompson, N. L. 1991. Topics in Fluorescence Spectroscopy Techniques. Plenum, New York.
47. Wu, J., A. H. Corbett, and K. M. Berland. 2009. The intracellular mobility of nuclear import receptors and NLS cargoes. *Biophys. J.* 96:3840–3849.
48. Van Craenenbroeck, E., J. Vercammen, …, Y. Engelborghs. 2001. Heuristic statistical analysis of fluorescence fluctuation data with bright spikes: application to ligand binding to the human serotonin receptor expressed in *Escherichia coli* cells. *Biol. Chem.* 382:355–361.
49. Macdonald, P., J. Johnson, …, J. D. Mueller. 2013. Brightness analysis. *Methods Enzymol.* 518:71–98.
50. Ferguson, S. M., and P. De Camilli. 2012. Dynamin, a membrane-remodelling GTPase. *Nat. Rev. Mol. Cell Biol.* 13:75–88.
51. Damke, H., T. Baba, …, S. L. Schmid. 1994. Induction of mutant dynamin specifically blocks endocytic coated vesicle formation. *J. Cell Biol.* 127:915–934.
52. Chen, H., S. Fre, …, P. De Camilli. 1998. Epsin is an EH-domain-binding protein implicated in clathrin-mediated endocytosis. *Nature.* 394:793–797.
53. Vieira, A. V., C. Lamaze, and S. L. Schmid. 1996. Control of EGF receptor signaling by clathrin-mediated endocytosis. *Science.* 274:2086–2089.
54. Sigismund, S., E. Argenzio, …, P. P. Di Fiore. 2008. Clathrin-mediated internalization is essential for sustained EGFR signaling but dispensable for degradation. *Dev. Cell.* 15:209–219.
55. Henriksen, L., M. V. Grandal, …, L. M. Grøvdal. 2013. Internalization mechanisms of the epidermal growth factor receptor after activation with different ligands. *PLoS One.* 8:e58148.
56. Müller, J. D., Y. Chen, and E. Gratton. 2000. Resolving heterogeneity on the single molecular level with the photon-counting histogram. *Biophys. J.* 78:474–486.

57. Takahashi, Y., N. Tsotakos, …, H.-G. Wang. 2016. The Bif-1-Dynamin 2 membrane fission machinery regulates Atg9-containing vesicle generation at the Rab11-positive reservoirs. *Oncotarget.* Published online March 10, 2016. http://dx.doi.org/10.18632/oncotarget.8028.

58. Goh, L. K., and A. Sorkin. 2013. Endocytosis of receptor tyrosine kinases. *Cold Spring Harb. Perspect. Biol.* 5:a017459.

59. Bitsikas, V., I. R. Corrêa, Jr., and B. J. Nichols. 2014. Clathrin-independent pathways do not contribute significantly to endocytic flux. *eLife.* 3:e03970.

60. Schmidt-Glenewinkel, H., E. Reinz, …, R. Eils. 2012. Multiparametric image analysis reveals role of Caveolin1 in endosomal progression rather than internalization of EGFR. *FEBS Lett.* 586:1179–1189.

61. Thoresen, S. B., N. M. Pedersen, …, H. Stenmark. 2010. A phosphatidylinositol 3-kinase class III sub-complex containing VPS15, VPS34, Beclin 1, UVRAG and BIF-1 regulates cytokinesis and degradative endocytic traffic. *Exp. Cell Res.* 316:3368–3378.

62. Rosenthal, J. A., H. Chen, …, P. De Camilli. 1999. The epsins define a family of proteins that interact with components of the clathrin coat and contain a new protein module. *J. Biol. Chem.* 274:33959–33965.

Biophysical Journal, Volume *111*

Supplemental Information

Association of Endophilin B1 with Cytoplasmic Vesicles

Jinhui Li, Barbara Barylko, John P. Eichorst, Joachim D. Mueller, Joseph P. Albanesi, and Yan Chen

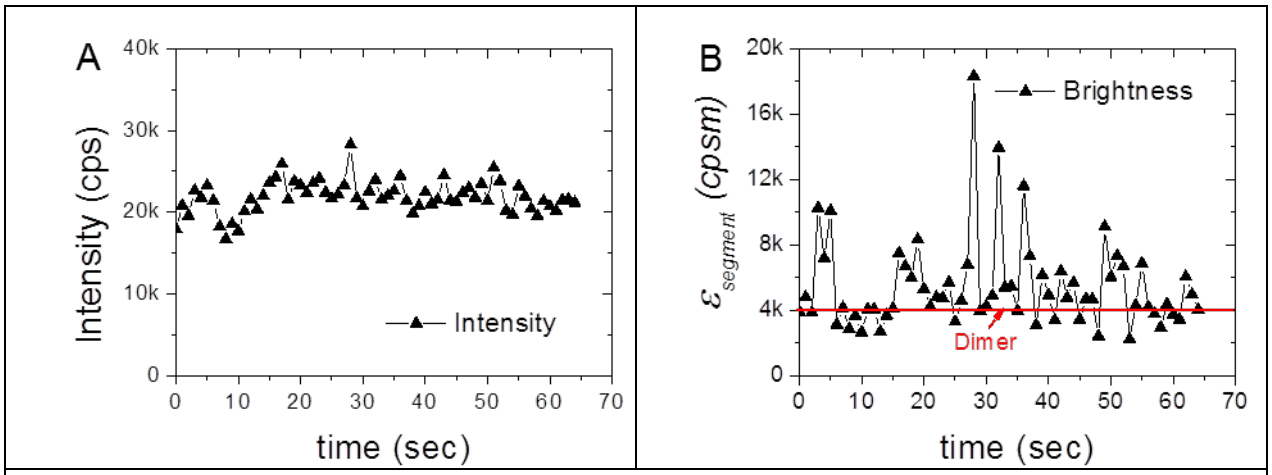

Figure S1. FFS data of EndoB1-GFP taken in an U2OS cell with a concentration of 110nM. (A) Fluorescence intensity trace and (B) segmented brightness determined by $\varepsilon_{segment}$ analysis. Dashed line indicates the calibrated dimer brightness for reference.

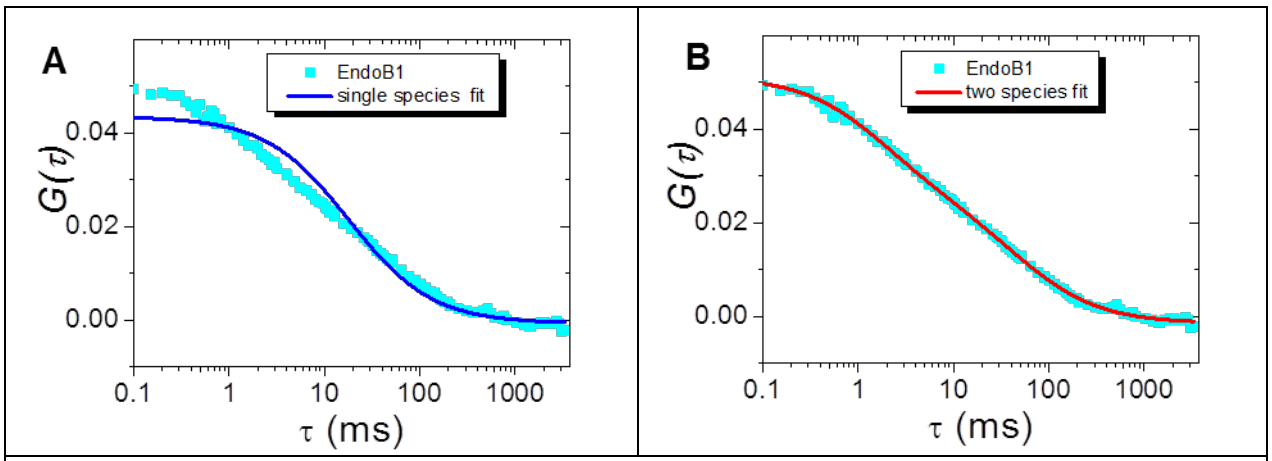

Figure S2. Autocorrelation of EndoB1-GFP taken in U2OS cell. (A) A fit (green line) to a single species model failed to describe the experimental autocorrelation (symbols). (B) The experimental data was fit to $a_1 f\left(t;\tau_1\right)+a_2 f\left(t;\tau_2\right)$ with $f\left(t;\tau\right)=\left(1+t/\tau\right)^{-1}$. The fit (red line) determined the residence times (τ_1 = 1.8 ms, τ_2 = 49.2 ms).

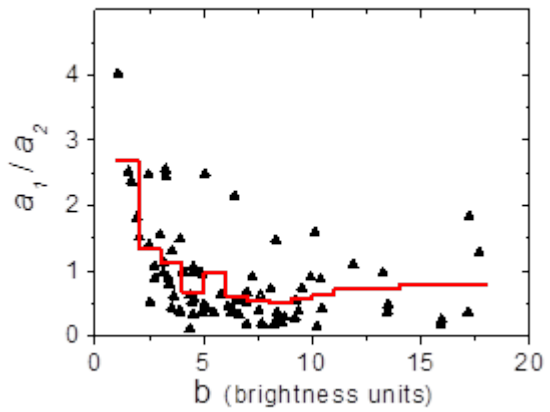

Figure S3. Amplitude ratio a_1/a_2 versus brightness b of EndoB1-GFP (▲). The mean-binned (n = 4, Δb = 1) amplitude ratio shown by the red line decreases with growing brightness and then plateaus.

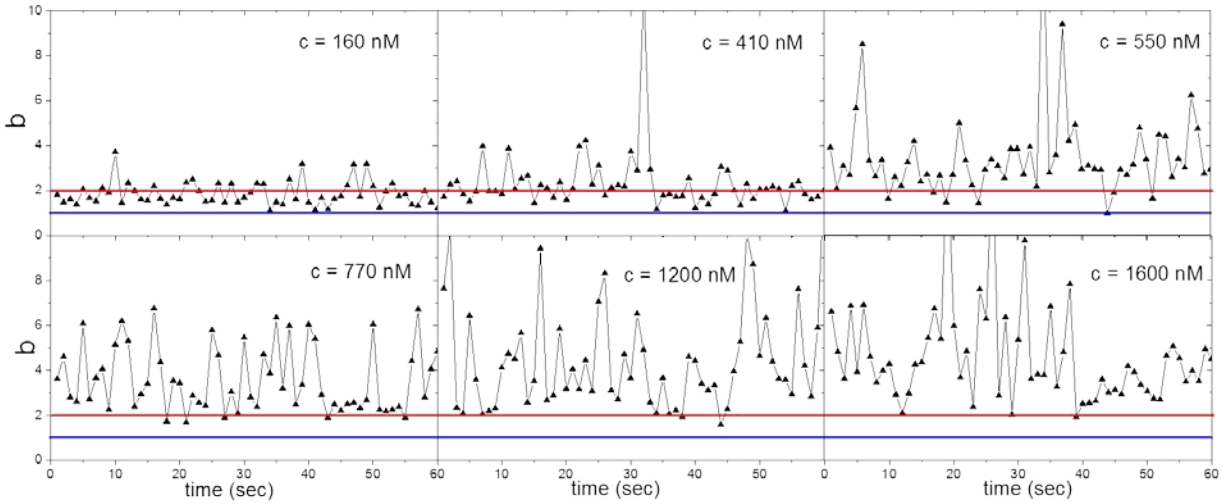

Figure S4. Segmented brightness b of EndoB1-GFP in U2OS cell. The segmented brightness is graphed for selected concentrations. The blue line indicates the monomeric brightness, and the red line identifies the dimeric brightness. The minimum of the segmented brightness of each graph falls in the range of monomeric to dimeric brightness.

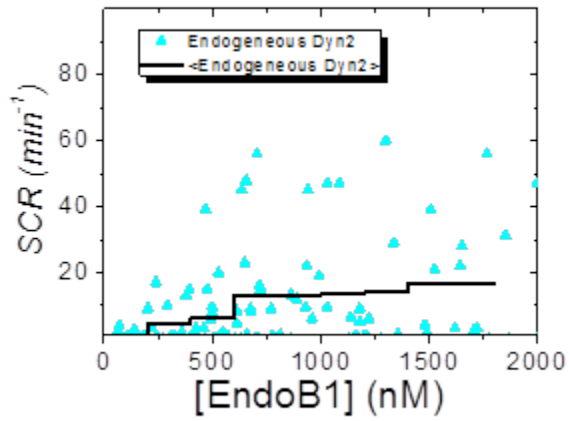

Figure S5. SCR of EndoB1 versus the labeled EndoB1 concentration in the presence of endogenous Dyn2. The mean (n = 6, Δc = 200 nM) of the binned spike count rate for EndoB1-GFP in the presence of endogenous Dyn2 is given by the black line.

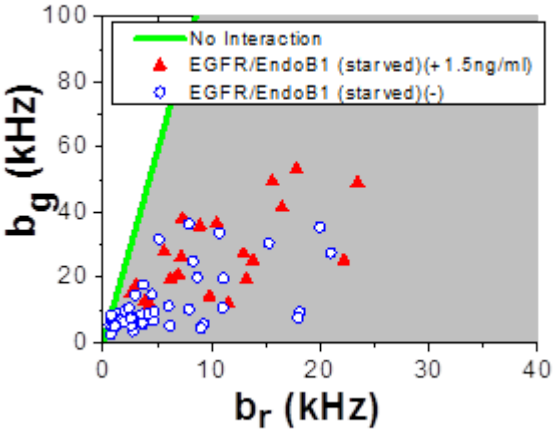

Figure S6. HSP brightness values for EGFR-EGFP and EndoB1-mCherry when serum starved for at least 4 hr (○) and after incubation with EGF (1.5 ng/ml) for 0.5 hr (▲).

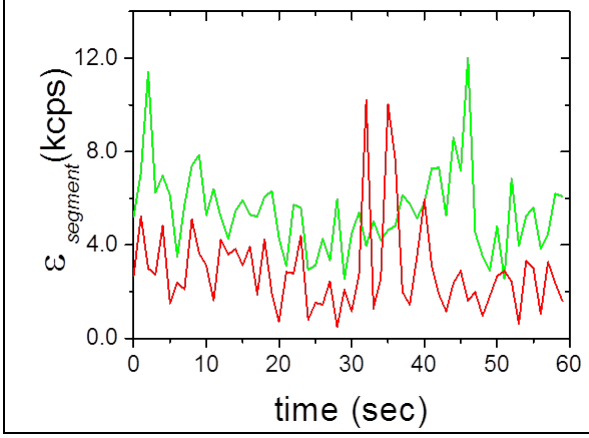

Figure S7. Segmented brightness plot of a U2OS cell expressing EndoB1-GFP and CLC-mCherry. The segmented brightness of the green detection channel (green line) and of the red detection channel (red line) is graphed versus time. The spikes in the red channel indicate the presence of CLC-mCherry containing vesicles, while the spikes in the green channel reflect the presence of vesicle-associated EndoB1-GFP. Brightness spikes in the two channels appear to be independent. The Pearson's correlation coefficient of the two data sets is 0.05.